

Star formation in distant starburst galaxies^{*}

C. Bonatto¹, E. Bica¹, M.G. Pastoriza¹, and D. Alloin²

¹ Universidade Federal do Rio Grande do Sul, IF, CP 15051, Porto Alegre 91501–970, RS, Brazil

² European Southern Observatory, Alonso de Cordova 3107, Santiago 19, Chile

Received 6 October 1999 / Accepted 7 January 2000

Abstract. This paper discusses the stellar population content of distant ($5\,000\text{ km s}^{-1} \leq V_R \leq 16\,000\text{ km s}^{-1}$) galaxies with enhanced star-formation activity. Distinction is made between isolated galaxies and galaxies morphologically disturbed, with clear signs of interaction such as mergers. In these galaxies the *International Ultraviolet Explorer (IUE)* large aperture samples most of the galaxy's body. Consequently, the resulting integrated spectra arise primarily from blue stellar populations of different ages together with significant contributions from intermediate and old age components, subject to varying reddening amounts. Instead of analysing individual, usually low Signal-to-Noise ratio (S/N) spectra, our approach is to coadd the spectra of objects with similar spectral properties in the UV, considering as well their properties in the visible/near-infrared ranges. Consequently, the resulting high (S/N) template spectra contain the average properties of a rather uniform class of objects, and information on spectral features can now be analysed with more precision. Three groups have been found for the interacting galaxies, corresponding to a red, blue and very blue continuum. Isolated galaxies have been separated into two groups, one with a flat/red continuum and the other with a blue continuum. For comparison, we also include in the present analysis two groups of nearby disturbed galaxies. Stellar populations are analysed by means of a synthesis algorithm based on star cluster spectral components of different ages which fit the observed spectra both in terms of continuum distribution and spectral features. Flux fractions of the different age groups found in the synthesis have been transformed into mass fractions, allowing inferences on the star formation histories. Young stellar populations (age $< 500\text{ Myr}$) are the main flux contributors, except for the groups with a red spectrum not due to extinction, arising from the intermediate (age $\approx 1 - 2\text{ Gyr}$) and old age populations. We also study the reddening values and the extinction law: a Small Magellanic Cloud-like extinction law is appropriate for all cases. As compared to nearby galaxies with enhanced star-formation, the distant starburst galaxy spectral groups exhibit larger contributions from the intermediate and old age populations. This effect is mainly accounted for by the larger spatial area sampled

by the *IUE* slit in the distant galaxies, including not only the entire bulge but also evolved disk populations. The present results provide a quantitative measure of the star-forming activity in interacting galaxies, compared to isolated galaxies.

Key words: galaxies: general – galaxies: interactions – galaxies: starburst – galaxies: stellar content – ultraviolet: galaxies

1. Introduction

Continuing our investigation of stellar populations in galaxies by means of a population synthesis algorithm based on ultraviolet (UV) spectra, in the present work we focus mainly on galaxy types with enhanced star-formation which are at distances corresponding to radial velocities in the range $5\,000\text{ km s}^{-1} \leq V_R \leq 16\,000\text{ km s}^{-1}$. Galaxies with clear signs of interactions such as those presenting a disturbed morphology, and particularly mergers, are studied and compared with similarly distant isolated galaxies, as well as with nearby disturbed galaxies.

Recently, the *International Ultraviolet Explorer (IUE) Satellite* database has been considerably improved in terms of spectra extractions, bad pixel corrections, calibrations, (S/N), etc, and its large aperture ($10'' \times 20''$) has provided a unique opportunity to understand integrated properties of galaxies in the UV in the local Universe.

Previous studies of galaxy spectra in the UV using *IUE* data have been carried out, e.g. the spectral atlases of Kinney et al. (1993) for star-forming galaxies, and Rosa et al. (1984) for H II complexes.

Ultraviolet spectra in the range $\lambda\lambda 1200 - 3200\text{ \AA}$ for a large number of galaxies with different morphologies can be retrieved from the *IUE* database. However, individual *IUE* spectra usually have a low (S/N), and a more useful approach is to group spectra of galaxies which share similar morphological and particularly, spectral properties in the UV. As a consequence, high (S/N) template spectra are thus obtained which represent the average properties of the galaxies making up the corresponding group.

Stellar population synthesis in the UV, using star cluster template spectra of different ages and metallicities as base elements, is a powerful tool to analyse the star-formation history of galaxies. The reason for this is that the variety of UV spectral

Send offprint requests to: C. Bonatto

^{*} Based upon data collected with the International Ultraviolet Explorer (*IUE*) Satellite, supported by NASA, SERC and ESA.

absorption features and continuum points measured in the star cluster components of the base, has been shown to be essentially age dependent (Bonatto et al. 1995, hereafter Paper I). A detailed description of the base of integrated star cluster spectra, including their age and metallicity properties, can be found in Paper I.

For the interpretation of the stellar population in the spectral groups obtained in the present work we use the population synthesis algorithm of Bica (1988), which was recently adapted to the UV range in a paper dealing with the analysis of *IUE* spectra of nearby spiral galaxies (Bonatto et al. 1998, hereafter Paper II). The base elements for the synthesis are the single-aged UV templates of stellar populations, i.e. the star cluster spectral groups defined in Paper I, as well as a bulge population template defined in Paper II.

The impact of different extinction laws is very marked, particularly in the UV, as denoted, for example, by the presence and strength of the $\lambda 2200 \text{ \AA}$ absorption feature associated to the dust. Thus, a proper determination of the stellar content of a galaxy allows, in turn, a correct determination of the reddening law affecting its stellar population. For this reason, in the synthesis procedure we test different reddening laws for the UV, including the Galactic, the Large and Small Magellanic Clouds (LMC and SMC) ones (Paper II; and Bonatto et al. 1996, hereafter Paper III).

The star cluster spectral base, together with the grouping procedure, have been extensively used in the investigation of the stellar populations in early-type galaxies (Paper III) and in the discussion of the UV-upturn phenomenon observed in some ellipticals (Bica et al. 1996). Besides, the stellar population synthesis has been fully explored in the investigation of the stellar content of nearby spiral galaxies (Paper II) and nearby magellanic and non-magellanic irregulars and nearby starburst galaxies (Bonatto et al. 1999, hereafter Paper IV).

This paper is organised as follows: in Sect. 2 we present the *IUE* data related to the sample galaxies. In Sect. 3 we group the objects according to spectral similarities from the UV to the visible/near-IR ranges. Equivalent width and continuum measurements are presented in Sect. 4. In Sect. 5 we study luminosity correlations among the different objects. The stellar population synthesis approach is introduced in Sect. 6, where we also discuss the synthesis results for each group. Concluding remarks are provided in Sect. 7.

2. The ultraviolet spectra

Data have been obtained from the *IUE* database at the *Space Telescope Science Institute* archives¹ and correspond to the *New Spectral Image Processing System* (NEWSIPS) re-processed spectra. We have selected the available low dispersion SWP, LWP and LWR spectra of the following objects: (i) – distant ($5\,000 \text{ km s}^{-1} < V_R \leq 16\,000 \text{ km s}^{-1}$) isolated galaxies, including compact and those classified as Blue Compact/H II galaxies; (ii) – distant luminous galaxies with different morphological peculiarities such as mergers, interacting galaxies,

highly disturbed galaxies, etc, i.e. all those types related to possibly enhanced star formation; and finally (iii) – nearby ($V_R \leq 5\,000 \text{ km s}^{-1}$) moderate-luminous disturbed galaxies (those not included in Paper IV). Only spectra obtained with the large *IUE* aperture ($10'' \times 20''$) have been considered.

Galaxies with normal stellar populations, i.e. those which do not show a clear sign of hosting an AGN, used in this work are presented in Table 1. Relevant data obtained mainly from de Vaucouleurs et al. (1991, hereafter RC3) and from the NASA/IPAC Extragalactic Database (NED)² are also included. We have gathered in Table 1 the following information on the sample galaxies, by columns: (1) most common name; (2) alternative identifications; (3) PGC number; (4) morphological type (T); (5) foreground absorption A_B ; (6) total blue magnitude B_T^0 ; (7) M_B assuming $H_0 = 75 \text{ km s}^{-1} \text{ Mpc}^{-1}$; (8) soft X-rays luminosity L_{SX} ; (9) $12\mu\text{m}$ luminosity $L_{12\mu\text{m}}$ obtained from IRAS fluxes given in NED; (10) far-IR luminosity L_{FIR} ³; (11) heliocentric radial velocity V_R ; and (12) complementary remarks. Absolute magnitudes M_B were calculated using Galactic Standard of Rest (V_G) velocities (RC3), while optical and H I heliocentric velocities (V_R) were considered for redshift corrections in the *IUE* spectra. The A_B values were used to correct all spectra for foreground (Galactic) reddening using Seaton’s (1979) law and adopting $A_B/E(B - V) = 4.0$. Thus, in the subsequent analyses all spectra are corrected for foreground reddening and for redshift. *Einstein Observatory* soft X-rays data in the range 0.2–4.0 keV have been taken mainly from Fabbiano et al. (1992); additional soft X-rays sources are from Wood et al. (1984) and Green et al. (1992).

For comparison purposes, we also make use in this paper of the objects and spectral groups (comprising nearby starburst and magellanic irregulars) presented in Paper IV.

3. Galaxy spectral groups

The stellar content, the physical state of the interstellar medium such as electron density, temperature, chemical composition, together with the amount of obscuring dust in a given galaxy, define the overall shape of its spectral energy distribution (SED). The UV spectral range seen with *IUE* between $\lambda\lambda 1200 - 3200 \text{ \AA}$ is particularly sensitive to the above parameters. However, the *IUE* spectra of individual normal stellar population galaxies in general have a low (S/N) which prevents a precise determination of these parameters. An alternative to individual galaxy studies is to analyse average properties of galaxies with similar morphological and, particularly, spectral parameters. On the one hand information on a particular object is lost, but on the other hand this procedure allows one to study the average properties of a large number of galaxies in more detail, from data with improved (S/N). In recent years, we have applied this method

² The NASA/IPAC Extragalactic Database (NED) is operated by the Jet Propulsion Laboratory, California Institute of Technology, under contract with the National Aeronautics and Space Administration.

³ $\log L_{FIR} = \log(2.58S_{60} + S_{100}) + 2 \log[z(1+z)] + 46.38$, where S_{60} and S_{100} are, respectively, the IRAS flux densities at 60 and $100\mu\text{m}$; z is the redshift.

¹ <http://archive.stsci.edu/iue/>

Table 1. Normal stellar population galaxies and corresponding groups

| Object | Other identifications | PGC # | T | A_B | B_T^0 | M_B | $\log L$ | | | V_R (km s^{-1}) | Remarks |
|---|--|----------|------|-------|---------|--------|------------------------|----------------------------------|---------------------------|---------------------------------|---------------------------|
| | | | | | | | S_X (L_\odot) | $12\mu\text{m}$ (L_\odot) | F_{IR} (L_\odot) | | |
| DISTANT ISOLATED GALAXIES | | | | | | | | | | | |
| <i>Group: G_Mrk1261 – Flat/red continuum</i> | | | | | | | | | | | |
| IC 1586 | Mrk 347, CGCG480-6, III Zw 012 | 2813 | — | 0.07 | 14.81 | -19.76 | — | <9.77 | 10.03 | 5821 | BCG, H II |
| Mrk 288 | MCG+12-14-13 | 53004 | — | 0.07 | 14.82 | -20.30 | — | 9.78 | 9.84 | 7500 | SBB? |
| Mrk 577 | UGC 1282 | 6694 | 0.0 | 0.15 | 13.73 | -20.65 | — | — | — | 5179 | S0/a |
| Mrk 1261 | UGC 5849, MCG+00-28-0003, ARK253 | 31998 | — | 0.16 | 13.99 | -21.22 | — | — | — | 7808 | Sc/d, H II |
| NGC 118 | Mrk 947, UM244, UGC 264, III Zw 9 | 1678 | 90.0 | 0.11 | 14.53 | -21.48 | <8.34 | 10.56 | 11.09 | 11250 | I0, compact |
| NGC 622 | Mrk 571, UM343, UGC 1143 | 5939 | 3.3 | 0.02 | 13.48 | -20.75 | — | <9.72 | 10.10 | 5161 | SBB |
| NGC 4156 | UGC 7173, MCG+7-25-0045 | 38773 | 3.0 | 0.00 | 13.79 | -20.99 | 8.13 | — | — | 6750 | SBB |
| NGC 4566 | UGC 7769 | 42007 | — | 0.00 | 13.55 | -20.75 | — | — | — | 5351 | S... |
| <i>Group: G_Mrk1267 – Blue continuum</i> | | | | | | | | | | | |
| Mrk 542 | UM191, CGCG382dd8 | 72998 | 10.0 | 0.08 | 15.80 | -19.27 | — | <10.04 | <9.97 | 7354 | Im, compact |
| Mrk 702 | PG 0842+162, IRAS 08427+1616 | 24616 | — | 0.09 | 15.70 | -21.00 | — | <10.41 | <10.76 | 15829 | compact, H II |
| Mrk 1267 | UGC 6003, MCG+01-28-0018, ARK264 | 32672 | — | 0.13 | 14.61 | -19.91 | — | — | — | 5780 | BCG |
| NGC 6062 | UGC 10202 | 57145 | 4.0 | 0.06 | 13.93 | -22.12 | — | 10.16 | 10.71 | 11717 | SBB |
| DISTANT INTERACTING GALAXIES | | | | | | | | | | | |
| <i>Group: G_N5860 – Red continuum</i> | | | | | | | | | | | |
| IC 214 | Mrk 1027, UGC 1720 | 8562 | — | 0.12 | 14.28 | -21.26 | — | 10.47 | 11.13 | 9061 | pair, pec |
| IC 4395 | Mrk 673, UGC 9141, IRAS 14156+2638 | 51033 | — | 0.00 | 14.42 | -21.41 | <7.53 | 10.24 | 11.06 | 10946 | S..., pair, H II |
| Mrk 499 | IZw166, CGCG252- 1 | 59028 | 10.0 | 0.00 | 15.30 | -19.80 | — | — | — | 7695 | Im, compact, pair |
| Mrk 789 | VIII Zw 323, IRAS 13299+1121 | 47623 | — | 0.00 | 14.50 | -21.00 | — | 10.25 | 10.96 | 9476 | Irr, pair, 2 nuclei, H II |
| NGC 828 | UGC 1655, VIZw177 | 8283 | 1.0 | 0.16 | 12.83 | -21.66 | — | 10.46 | 11.05 | 5374 | Sa:, pec, merger, H II |
| NGC 2623 | UGC 4509, ARP 243 | 24288 | 99.0 | 0.09 | 13.07 | -21.33 | — | 9.99 | 11.31 | 5535 | triple, merger |
| NGC 5860 | Mrk 480, UGC 9717, IZw102 | 53939 | — | 0.04 | 14.20 | -20.17 | — | 9.72 | 10.20 | 5398 | merging pair, pec, S? |
| <i>Group: G_N4410 – Blue continuum</i> | | | | | | | | | | | |
| IC 298 | MCG+00-9-16, in ARP 147, VV787, IZw11 | 11890 | 10.0 | 0.24 | 15.50 | -20.29 | — | <10.25 | 10.44 | 9656 | merger, ring, pair, H II |
| NGC 4410 | VCC904 | 40694 | 2.0 | 0.00 | 14.01 | -20.89 | 7.95 | — | — | 7252 | double, in contact |
| NGC 6090 | Mrk 496a, UGC 10267 | 57437 | — | 0.00 | 14.00 | -21.38 | 8.02 | 10.50 | 11.18 | 8785 | pair, merger, 2 nuclei |
| NGC 7609B | MCG+01-59-47, ARP 150 | 71076 | 99.0 | 0.14 | 14.59 | -21.58 | — | — | — | 11885 | pair |
| <i>Group: G_Mrk54 – Very blue continuum</i> | | | | | | | | | | | |
| ESO 185-IG13 | IRAS 19410-5422 | 63618 | — | 0.19 | 14.83 | -19.72 | — | <9.49 | <9.85 | 5600 | compact, pec, H II |
| ESO 296-IG11 | Ag6, VV578, AM0117-412 | 4792 | — | 0.03 | 14.34 | -20.02 | — | <9.55 | 9.93 | 5572 | double, group |
| ESO 350-IG38 | IRAS 00344-3349 | 2204 | — | 0.02 | 14.18 | -20.40 | <7.82 | 10.33 | 10.77 | 6156 | double, merging, H II |
| ESO 400-G43 | Frl1165 | 65093 | — | 0.09 | 14.13 | -20.49 | — | 9.71 | 10.18 | 5900 | pair, pec, compact, H II |
| ESO 462-IG20 | IRAS 20239-2916 | 64707 | — | 0.29 | 14.42 | -20.39 | — | <9.77 | <9.79 | 6030 | double, contact |
| Mrk 26 | UGC 5491, MCG+10-15-26 | 29697 | 4.5 | 0.00 | 15.86 | -19.58 | — | <9.98 | 10.02 | 9122 | Sb/c?, pair |
| Mrk 54 | IRAS 12546+3243, MCG+06-28-44 | 44213 | 5.0 | 0.03 | 14.75 | -21.55 | — | <10.39 | 10.78 | 13421 | Sc, triple, BCG, H II |
| Mrk 66 | MCG+10-19-72 | 46988 | — | 0.01 | 15.00 | -19.74 | — | <9.80 | 9.85 | 6525 | pair, BCG |
| Mrk 220S | UGC 7905, MCG+09-21-34 | 42844 | — | 0.00 | 14.70 | -19.40 | — | — | 10.13 | 4875 | pair, BCG, pec, interac |
| NGC 6240 | UGC 10592, IRAS 16504+0228 | 59186 | 90.0 | 0.31 | 13.48 | -21.79 | 8.94 | 10.62 | 11.54 | 7339 | I0, pec, merger |
| NEARBY DISTURBED GALAXIES | | | | | | | | | | | |
| <i>Group: G_N4438 – Bulge stellar population and moderate UV</i> | | | | | | | | | | | |
| ESO 383-G35 | MCG-06-30-015, IRAS 13329-3402 | 47969 | — | 0.12 | 13.45 | -19.02 | 9.02 | 9.40 | 9.13 | 2323 | S?, in cluster |
| NGC 4438 | UGC 7574, VCC1043, in ARP 120 | 40914 | .0 | 0.10 | 10.59 | -21.21 | 7.26 | 8.79 | 9.64 | 71 | SA0/a pec, pair |
| <i>Galaxy: ESO 338IG4 – Very blue starburst with emission lines</i> | | | | | | | | | | | |
| ESO 338-IG4 | IRAS 19245-4140, Tol 1924-416 | 63240 | — | 0.32 | 13.44 | -19.79 | — | <8.89 | 9.49 | 2874 | BCG, pec, H II |

Table notes. S_X , $12\mu\text{m}$ and F_{IR} in Columns (8), (9) and (10) are, respectively, the logarithm of the *Einstein Observatory* 0.2–4.0 keV soft X-rays, $12\mu\text{m}$ and far-IR (60–100 μm) IRAS luminosities in solar units.

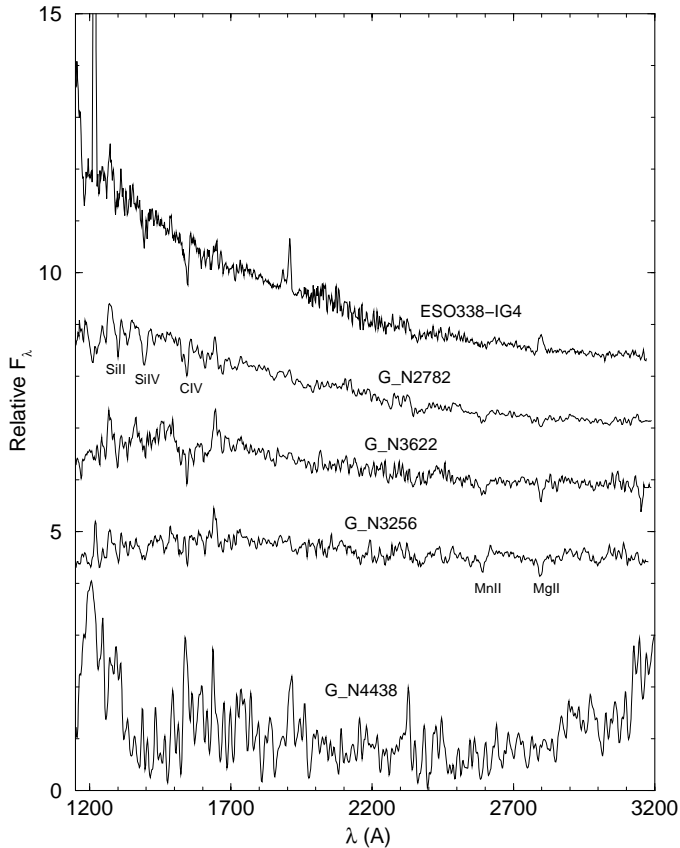


Fig. 1. Nearby disturbed galaxy groups. The luminous starbursts of Paper IV (G_N2782, G_N3622 and G_N3256) are also shown for comparison purposes. Some absorption features are indicated. Flux in F_λ units, normalised at $\lambda 2646 \text{ \AA}$. Constants have been added to the spectra for clarity purposes, except for the bottom one.

to analyse a number of different objects: early-type galaxies, both normal and active (Paper III and Bica et al. 1996); white dwarf stars (Bica et al. 1996); nearby spiral galaxies (Paper II); and magellanic and non-magellanic irregulars and H II galaxies (Paper IV).

In order to obtain such data and to analyse the UV SED and spectral features it is necessary first to coadd the available *IUE* spectra of each individual object, and subsequently to coadd into a spectral group the spectra of objects which show morphological and spectral similarities. In the present grouping procedure the ultimate criterion is the similarity of the UV spectra at the available (S/N). However, we also consider the spectral properties in the visible and near-IR ranges derived from the literature, together with the classifications as H II galaxy, starburst or usual normal stellar population types (Table 1). To do this we have used information from the following references, which were useful for classification according to stellar population and/or emitting gas characteristics: Heckman et al. (1980); Caldwell (1984); Dahari (1985); Filippenko & Sargent (1985); Bica & Alloin (1987a, 1987b); Davies et al. (1987); Bettoni & Buson (1987); Gregg (1989); Bonatto et al. (1989); Terlevich et al. (1991); Bica et al. (1991); Buson et al. (1993); Storchi-Bergmann et al. (1995).

Three steps were taken to build up the final spectral groups: (i) we averaged individual *IUE* spectra of a given object working separately in the short (SWP) and long (LWP and LWR) wavelength ranges. A few spectra were eliminated at this stage because they presented problems such as instrumental defects, discordant continuum distribution and/or spectral features; (ii) we coadded spectra of different objects with comparable spectral properties — the ultimate criterion being the spectral similarity in the UV, in particular the continuum shape and the strength of the lines; and (iii) the short and long wavelength domains were finally connected. The weight of each spectrum in the average was attributed according to the square of the (S/N).

In Table 1 we present the resulting spectral groups, along with the galaxies they are made of. Each spectral group is named after a member which has spectra both in the SWP and LWP/LWR domains with a good (S/N). Average properties for each group are given in Table 2, in which the average projected *IUE* aperture in kpc (Column 6) is also included. Data for the nearby magellanic irregular and starburst galaxy groups of Paper IV are also displayed in Table 2.

The groups with nearby ($V_R \leq 5000 \text{ km s}^{-1}$) disturbed galaxies are shown in Fig. 1, together with the luminous starburst groups studied in Paper IV. Notice the presence of emission lines in the spectrum of ESO 338-IG4. Groups with distant ($5000 \text{ km s}^{-1} \leq V_R \leq 16000 \text{ km s}^{-1}$) normal stellar population galaxies are shown in Fig. 2: interacting galaxies are in the top panel and isolated galaxies are in the bottom panel.

Finally we note that the galaxies in each group have similar absolute magnitudes which basically precludes the possibility of considerable metallicity differences among galaxies in a given group. We recall that in Paper IV we dealt with dwarf and giant galaxy groups, and consequently the fact that in that paper we kept galaxies separated by absolute magnitude naturally separated them by metallicity.

4. Equivalent width and continuum measurements

The stellar population analysis to be performed on the present group spectra is based on the measured equivalent width (EW) of selected absorption features and on measured continuum points. These spectral windows and continuum regions in the UV have been previously defined in Paper I. In Table 3 we present the EWs and continuum points (normalised at $\lambda 2646 \text{ \AA}$) measured for the normal stellar population groups. The identification number and wavelength limits of the UV windows (according to the definition in Paper I), together with the main contributing absorbers in each window, are given in Columns (1) – (3) of Table 3. Note that these absorption lines are primarily of stellar origin, although some interstellar contribution cannot be excluded (Paper I).

5. Sample characterisation

Before analysing the UV spectra in detail, we can use the individual galaxy luminosities listed in Table 1, and the group averages in Table 2, to investigate the global properties of our sam-

Table 2. Average Properties

| Group/ Object | $\langle M_B \rangle$ | $\log L (L_\odot)$ | | | $\langle 10'' \rangle$ (kpc) |
|-------------------------------------|-----------------------|--------------------------|----------------------------|--------------------------|---------------------------------|
| | | $\langle S_X \rangle$ | $\langle 12 \mu m \rangle$ | $\langle F_{IR} \rangle$ | |
| <i>Nearby Disturbed Galaxies</i> | | | | | |
| G_N4438 | -20.11 ± 1.54 | 8.14 ± 1.24 | 9.09 ± 0.43 | 9.38 ± 0.36 | 1.24 ± 0.26 |
| G_N3256 | -20.06 ± 0.68 | $< 8.05 \pm 0.97$ | 9.69 ± 0.41 | 10.14 ± 0.53 | 2.35 ± 0.47 |
| G_N3622 | -20.07 ± 0.91 | $< 7.56 \pm 0.54$ | $< 9.57 \pm 0.73$ | 10.18 ± 0.79 | 2.11 ± 0.73 |
| G_N2782 | -19.32 ± 1.42 | $< 7.33 \pm 0.07$ | $< 9.31 \pm 0.70$ | 9.92 ± 0.93 | 1.89 ± 0.64 |
| ESO 338-IG4 | -19.79 | — | < 8.89 | 9.49 | 1.85 |
| <i>Nearby Magellanic Galaxies</i> | | | | | |
| G_N1313 | -17.06 ± 1.66 | $\lesssim 5.61 \pm 0.73$ | $< 7.88 \pm 0.73$ | $\lesssim 8.61 \pm 0.67$ | 0.54 ± 0.32 |
| G_N4449 | -16.72 ± 1.94 | $\lesssim 5.68 \pm 1.13$ | $< 7.52 \pm 0.94$ | $\lesssim 8.12 \pm 1.00$ | 0.51 ± 0.46 |
| <i>Distant Isolated Galaxies</i> | | | | | |
| G_Mrk1261 | -20.74 ± 0.53 | $< 8.23 \pm 0.14$ | $< 9.96 \pm 0.40$ | 10.26 ± 0.56 | 4.47 ± 1.33 |
| G_Mrk1267 | -20.57 ± 1.25 | — | $< 10.20 \pm 0.18$ | $< 10.48 \pm 0.44$ | 6.57 ± 2.92 |
| <i>Distant Interacting Galaxies</i> | | | | | |
| G_N5860 | -20.95 ± 0.69 | < 7.53 | 10.19 ± 0.28 | 10.95 ± 0.38 | 4.97 ± 1.45 |
| G_N4410 | -21.03 ± 0.57 | 7.98 ± 0.05 | $< 10.37 \pm 0.17$ | 10.81 ± 0.52 | 6.11 ± 1.30 |
| G_Mrk54 | -20.31 ± 0.80 | $< 8.38 \pm 0.79$ | $< 9.96 \pm 0.39$ | 10.34 ± 0.57 | 4.58 ± 1.63 |

Table notes. Data for the nearby starburst (G_N3256, G_N3622 and G_N2782) and magellanic irregular (G_N1313 and G_N4449) groups of Paper IV are also given; F_{IR} refers to the IRAS 60–100 μm luminosity.**Table 3.** Equivalent width and continuum measurements

| UV# | Window (\AA) | Main absorbers | G_N4438 | ESO 338-IG4 | G_Mrk1261 | G_Mrk1267 | G_N5860 | G_N4410 | G_Mrk54 |
|----------------------------|---|----------------------|------------------------------------|-------------|-----------|-----------|---------|---------|---------|
| | | | Equivalent Widths (\AA) | | | | | | |
| 4 | 1290–1318 | Si II, Si III | 4.20 | 3.34 | 9.12 | 7.20 | 4.47 | 6.19 | 4.12 |
| 7 | 1384–1414 | Si IV, Fe V | 10.00 | 4.42 | 3.00 | 3.69 | 4.34 | 5.04: | 5.36 |
| 13 | 1534–1570 | C IV | † | 4.66 | 6.60: | 8.07 | 7.07 | † | 5.33 |
| 19 | 1700–1736 | N IV, Si IV, Fe IV | 8.12 | 2.54 | 2.50: | 1.95: | 1.48 | 0.30: | 1.58 |
| 43 | 2506–2574 | Fe I, Si I, Si III | 24.75 | 7.67 | 11.64 | 12.59 | 7.38 | 20.23 | 9.60 |
| 44 | 2574–2596 | Mn II, Fe II | 13.87 | 3.62 | 10.62 | 5.72 | 8.07 | 12.24 | 7.32 |
| 45 | 2596–2642 | Fe II, Mn II, Si III | 14.56 | 4.17 | 28.11 | 3.99 | 6.88 | 17.75 | 7.82 |
| 51 | 2768–2830 | Mg II, Mn II, O V | 25.14 | † | 28.22 | 11.86 | 17.28 | 21.72 | 14.95 |
| 52 | 2830–2900 | Mg I, C II, Si I | 20.33 | † | 9.43: | 12.11 | 16.89 | 28.27: | 13.68 |
| λ (\AA) | Continuum points – C_λ/C_{2646} | | | | | | | | |
| 1282 | | | 2.12 | 4.55 | 1.09 | 2.95 | 0.62 | 1.72 | 3.67 |
| 1348 | | | 1.31 | 3.89 | 0.89 | 2.92 | 0.60 | 1.56 | 3.38 |
| 1490 | | | 1.55 | 3.33 | 1.10 | 2.62 | 0.75 | 1.57 | 3.18 |
| 1768 | | | 1.54 | 2.33 | 1.00 | 2.07 | 0.65 | 1.26 | 2.16 |
| 2079 | | | 0.93 | 1.80 | 1.05 | 1.56 | 0.82 | 0.95 | 1.68 |
| 2258 | | | 0.77 | 1.33 | 0.96 | 1.28 | 0.86 | 0.86 | 1.35 |
| 2466 | | | 0.95 | 1.17 | 0.94 | 1.05 | 0.85 | 0.86 | 1.09 |
| 2959 | | | 1.38 | 0.77 | 1.88 | 0.95 | 1.04 | 1.06 | 1.02 |
| 3122 | | | 1.88 | 0.78 | 2.40 | 1.06 | 1.22 | 1.15 | 1.03 |

Table notes. Uncertainties in EWs are typically $\leq 10\%$, except for G_N4438 for which they may be as high as 40%; † – Emission line contamination.

ple. In the four panels of Fig. 3 we investigate relations between the soft X-rays, 12 μm and far-IR (60–100 μm) luminosities and absolute B magnitude for our normal galaxies. We remind that data for the nearby magellanic irregulars and the nearby luminous starbursts – except ESO 338-IG4 and G_N4438 – are

from Paper IV. As expected for these normal stellar population galaxies, the absolute B magnitude correlates well both with the soft X-rays (bottom-left panel) and the IRAS far-IR (upper-left panel) luminosities. The reason for this is that X-rays originate mainly from phenomena such as supernovae explosions and

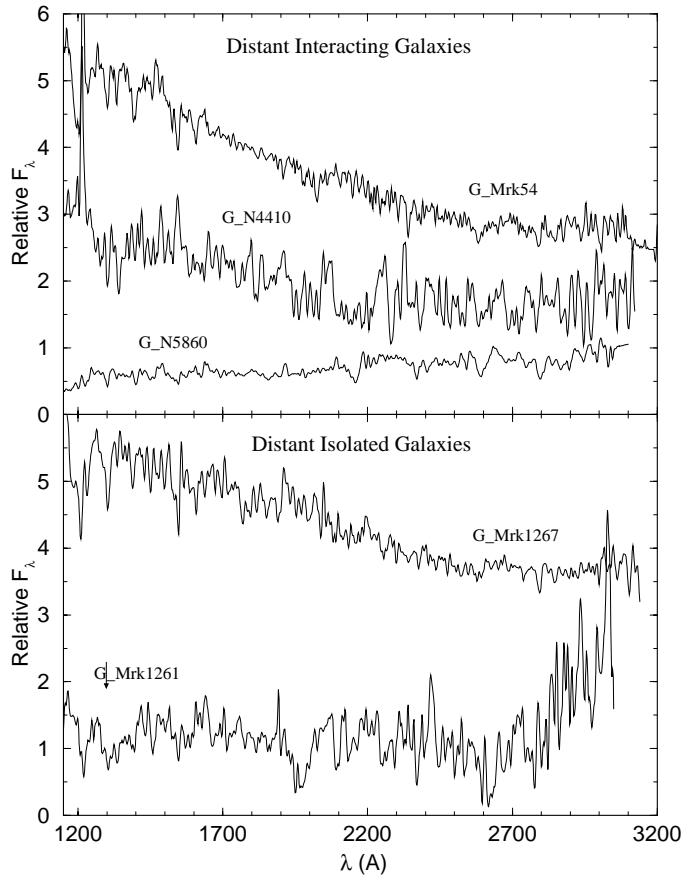


Fig. 2. Same as Fig. 1 for the distant ($V_R > 5000 \text{ km s}^{-1}$) galaxy groups. Top panel: groups of interacting galaxies. Bottom panel: groups of isolated galaxies.

Wolf Rayet stars, i.e., processes strongly associated to recent star formation; the infrared dust emission is also associated to recent star formation, in particular in the $60\text{--}100\mu\text{m}$ wavelength region.

Stellar population syntheses performed on the nearby luminous starbursts and magellanic irregulars revealed the presence of enhanced recent star formation (Paper IV). As also shown in Fig. 6 of Paper IV, the UV spectra of the nearby magellanic irregulars present evidence of shock-heated gas from supernovae explosions as denoted by a series of semi-forbidden lines, while the luminous starbursts show evidence of photoionisation by very hot stars (or even a low-luminosity AGN). Similar results, with respect to recent star formation, are also obtained for the sample galaxies studied in the present paper (Sect. 6). At any rate, in both luminosity classes we are observing indicators of the star-formation activity. As a consequence, in the absence of an important nuclear source of high energy photons such as an AGN, the X-rays and IR luminosities should scale up with galaxy mass for such star-forming galaxies, similarly to M_B . This is confirmed by the good correlations between the soft X-rays and $12\mu\text{m}$ (Fig. 3, bottom-right panel) and soft X-rays and IRAS far-IR (Fig. 3, upper-right panel) luminosities.

Leitherer et al. (1995) showed that the absorption features $\text{Si IV}_{\lambda 1400}$ and $\text{C IV}_{\lambda 1549}$ are very sensitive indicators of the

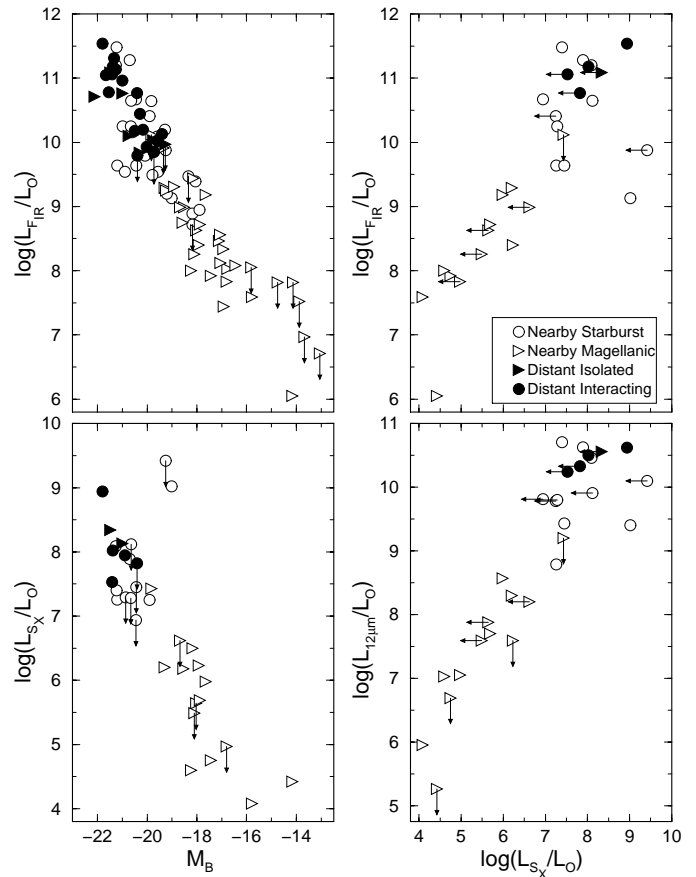


Fig. 3. Luminosity data for the normal stellar population galaxies. L_{FIR} is the IRAS $60\text{--}100\mu\text{m}$ luminosity. Arrows indicate upper limits.

presence of young, massive O and B stars. The link between recent star formation and the $12\mu\text{m}$ luminosity is further indicated for our sample objects, as can be seen in Fig. 4 where we have plotted, for each group of isolated and interacting galaxies, the average values of the EW of C IV (Table 3) and $12\mu\text{m}$ luminosity (Table 2). Since the $12\mu\text{m}$ emission correlates with that of the soft X-rays (Fig 3, bottom-right panel), the soft X-rays luminosity also correlates with EW(C IV).

Helou (1986, see also Boulanger et al. 1988) studied the IRAS colour ratios ($12/25\mu\text{m}$ and $60/100\mu\text{m}$) for normal galaxies including both star-forming and quiescent (cirrus dominated) ones. He concluded that the far-infrared luminosity is not simply proportional to the number of massive young stars in a normal galaxy. Note, however, that our sample consists essentially of *star-forming galaxies* as becomes clear in the population syntheses in Sect. 6 together with the galaxy groups from Paper IV, as a consequence of the natural bias in the IUE galaxy sample which in general preferred galaxies with UV excess. The present results and Helou's are thus not at odds, and the present sample suggests that *among star-forming galaxies* the luminosity should scale with mass. Small dust grains are likely to be destructed by intense radiation fields associated to active star-forming environments which would decrease the $12\mu\text{m}$ luminosity. However, the present sample of star-forming

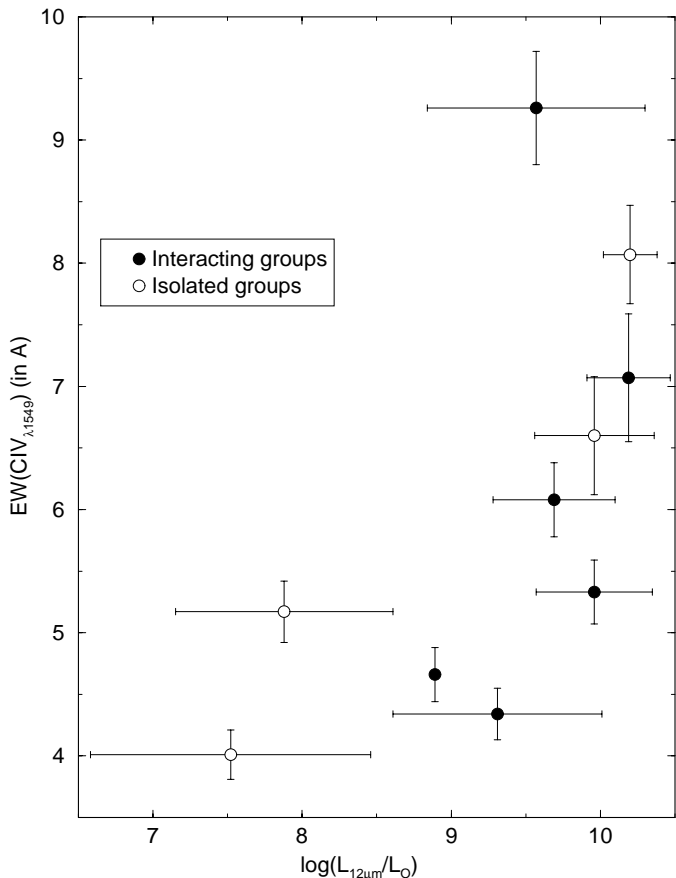


Fig. 4. The $12\mu\text{m}$ luminosity correlates with the $\text{EW}(\text{C IV}_{\lambda 1549})$, which is related to recent star formation. The points correspond to the internal averages within each group, and the bars are the corresponding standard deviations.

galaxies suggests that overall bursts in a galaxy, observed in large apertures such as that of IUE, still have important $12\mu\text{m}$ flux, arising from relatively hot dust shielded from the radiation field and possibly with some contribution from cool supergiants.

According to Table 2, for each galaxy group the *IUE* aperture samples large spatial regions and, therefore, the observed spectrum should contain contributions from different stellar populations. In Fig. 5 we investigate this effect on the EW of absorption features primarily arising from young (e.g. $\text{C IV}_{\lambda 1549}$) and old (e.g. $\text{Mg II}_{\lambda 2800}$) stellar populations (Paper I). The result for C IV , in the bottom panel of Fig. 5, seems to indicate a cumulative effect, such as would occur in the case of large-scale star formation. In particular, this cumulative effect is related to the increasing sampling of disk regions.

As shown in Paper I (and also in Table 8 of Paper II), there is a strong dependency of $\text{EW}(\text{Mg II}_{\lambda 2800})$ on stellar population age, in the sense that older populations have larger EWs. Thus, the large $\text{EW}(\text{Mg II}_{\lambda 2800})$ measured in G_Mrk1261, G_N4438, G_N4410 and G_N5860 (Fig. 5, top panel), suggests the presence of old stellar populations. In fact, according to the present stellar population synthesis (Sect. 6 and Table 4), these are the groups with the largest flux contribution from the intermediate (age ≈ 1.2 Gyr) and old age populations.

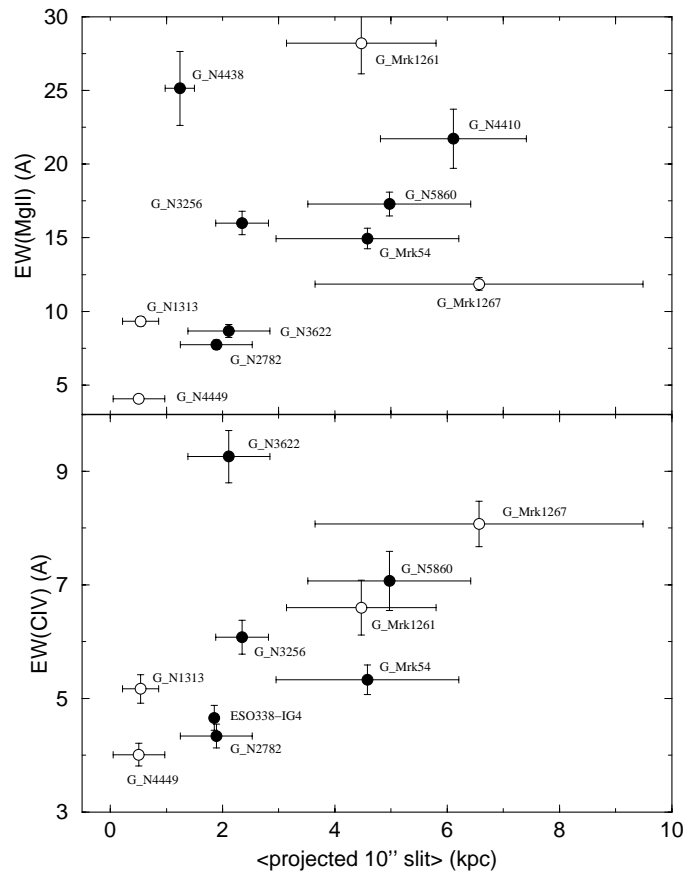


Fig. 5. Effect of varying the spatial regions included on the slit. Top panel: $\text{EW}(\text{Mg II}_{\lambda 2800})$; the groups G_Mrk1261, G_N4438, G_N4410 and G_N5860 have the largest flux contribution from the intermediate and old age populations. Bottom panel: same as above for the $\text{EW}(\text{C IV}_{\lambda 1549})$.

It is interesting to note that galaxies with signs of interaction (including mergers and disturbed galaxies) are located on the high-end of the luminosity range.

6. Stellar population synthesis

Stellar population synthesis is better constrained when one considers a wavelength range as wide as possible, as emphasised already by e.g., Bica (1988) and Alloin & Bica (1990). As shown in Paper II for spiral galaxies, synthesis in the UV range is well constrained because of the marked variety of spectral features and continuum distribution occurring in the star cluster components in the UV range, which are predominantly age dependent (Paper I). For this reason, the simplest approach is to perform an independent population synthesis in the UV range alone, and apply the same method to all groups.

Following Bica (1988) and Schmitt et al. (1996), we have adapted the population synthesis algorithm to the UV range in Paper II. Basically this algorithm uses EWs of the most prominent absorption features and selected continuum points observed in a given spectrum, and compares them to those of a model computed from a base of simple stellar population ele-

Table 4. Stellar population synthesis results

| Group | $\lambda 2646 \text{ \AA}$ Flux fraction (in%) | | | | | | | $E(B - V)^\ddagger$ |
|-------------|--|------------------|-----------------|------------------|-------------------|--------------------|------------------|---------------------|
| | Element: Age: | RH II 2.5 Myr | LMC I 10 Myr | LMC II 25 Myr | LMC III 75 Myr | LMC IVA 200 Myr | LMC V 1.2 Gyr | |
| G_N4438 | 8.23 | 10.20 | 13.25 | 5.30 | 4.16 | 3.37 | 55.49 | 0.00 |
| ESO 338-IG4 | 45.12 | 41.11 | 8.26 | 1.61 | 1.14 | 1.90 | 0.87 | 0.00 |
| G_Mrk1261 | 15.35 | 3.51 | 6.14 | 3.80 | 2.12 | 2.20 | 66.88 | 0.07 |
| G_Mrk1267 | 35.53 | 5.19 | 15.21 | 21.44 | 12.34 | 1.37 | 8.91 | 0.01 |
| G_N5860 | 1.00 | 31.25 | 6.08 | 2.50 | 1.42 | 57.75 | <0.01 | 0.14 |
| G_N4410 | 4.97 | 27.89 | 12.22 | 5.11 | 8.56 | 33.09 | 8.16 | 0.04 |
| G_Mrk54 | 53.71 | 4.30 | 8.89 | 14.32 | 5.87 | 1.74 | 11.16 | 0.00 |

Table notes. \ddagger - Reddening-corrected using an SMC law.

ments. The algorithm is not a minimisation procedure, instead it generates all possible combinations of the base elements according to a given flux contribution step and compares the resulting EWs and continuum points to the input ones. The code successively de-reddens galaxy input continuum points and tests them against a given model generated from the base elements. The acceptable solutions, within error bars, are averaged out: this average is adopted as the final synthesis solution.

The IUE is well-known to have a low-response in the region $\approx \lambda 2000 - 2300 \text{ \AA}$, and we do not include this region in the syntheses. Well-known spikes have also been taken into account at observed wavelengths (Paper I). Redshift corrections further ensure the real nature of spectral features in groups spectra, averaging out eventual detector deficiencies (Papers II, III and IV).

The base elements that we use in the present UV synthesis are taken from the star cluster population templates described in Paper I to represent young (including an H II region template) and intermediate age components, and a galaxy template taken to represent an old metal-rich bulge (Paper III). EWs and continuum points of the H II region element were measured on the average spectrum of the M 101, M 33, LMC and SMC groups from Paper I. For young and intermediate age elements, we use LMC star cluster groups with ages $\approx 10, 25, 75, 200$ and 1200 Myr (respectively the groups I, II, III, IVA and V in Paper I). Finally, we use a bulge template (named E2E5 by Bica and collaborators – see the database in Leitherer et al. 1996), which is the average of the far-UV weak elliptical galaxy groups G_N1553 and G_N3115 (Paper III). EWs and continuum points for these base elements are listed in Table 8 of Paper II.

All synthesis runs included the 7 age components described above. Initially, we used a 5% step for testing flux contributions at $\lambda 2646 \text{ \AA}$, generating 230 230 combinations for each assumed $E(B - V)$. Typically, for the appropriate $E(B - V)$, only 5% of these 230 230 element combinations are acceptable solutions within the error windows. Reddenings were tested in the range $0.0 < E(B - V) < 0.5$ with a step of $\Delta E(B - V) = 0.01$. Thus, in total, $\approx 1.15 \times 10^7$ element combinations are tested for each group, and acceptable solutions amount to less than 1%. Finally, after having probed as above a large space of com-

binations, we calculate the final solution with finer steps (2% in flux contributions).

The Galactic (Seaton 1979), LMC (Fitzpatrick 1986) and SMC (Prévot et al. 1994) reddening laws have been tested in the synthesis of each group.

It is interesting to point out that a very reddened blue stellar population cannot be confused with a red (predominantly old and/or intermediate age) stellar population because there are spectral features which differ considerably in strength (Paper I), such as those in windows 44 (Fe II) and 45 (Mg II). Compare also the typically blue and red stellar populations respectively of G_Mrk1261 and G_Mrk1267 (Fig. 9) and their EW values in Table 3.

Synthesis results for the present normal stellar population galaxy groups are given in Table 4 where we present the percentage flux contribution of each base element to the group stellar population, at $\lambda 2646 \text{ \AA}$; $E(B - V)$ values are also given in the table, using the SMC extinction law. It is interesting to point out that in no case Seaton's Galactic reddening law can be applied to correct for the internal reddening of these galaxies, such a correction producing prohibitive flux excesses in the region around $\lambda 2200 \text{ \AA}$. A similar result has been found for the sample of normal nearby spirals in which there are cases where an SMC reddening law applies and cases where an LMC law applies (Paper II). The same conclusion was reached by Kinney et al. (1994). For the enhanced star formation galaxies of Paper IV, only the SMC extinction law applies.

Extragalactic reddening laws for extended objects seem to work differently than interstellar ones deduced from stars (Calzetti et al. 1994), so that the term attenuation is often used now in place of extinction when referring to the loss of light in a galaxy spectrum due to intervening dust mixed with the stars. The latter extragalactic obscuration law (EOL) was compared to the LMC and SMC laws (deduced from stars) in Fig. 1 of Calzetti et al. (1995). The EOL on average follows the LMC curve, except that it presents no $\lambda 2200 \text{ \AA}$ bump. In this respect it is similar to the SMC curve, which however is steeper. As a consequence, the application of the EOL curve to the present spectra would produce similar results (i.e. SMC law, absence of bump), but the associated colour excesses $E(B - V)$ would be somewhat higher.

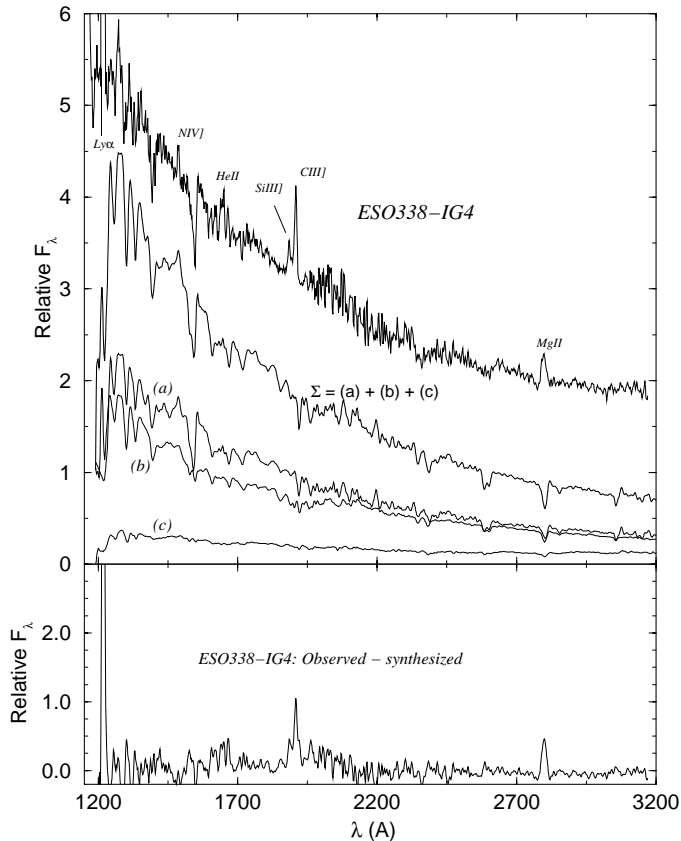


Fig. 6. Top panel: synthesis of ESO 338-IG4, the nearby starburst galaxy with blue continuum and emission lines. Components are: (a) – H II region; (b) – LMC I; (c) – sum of LMC II, LMC III, LMC IVA, LMC V and E2E5. The main emission-lines are indicated. The spectra are shown in their true proportion according to the synthesis, except that a constant has been added to the top one (observed galaxy spectrum) for clarity purposes. The spectrum shown with bold line is the synthesized one. Bottom panel: resulting pure-emission spectrum of ESO 338-IG4, observed – synthesized.

The synthesis procedure is illustrated in detail in Fig. 6 for the nearby starburst galaxy ESO 338-IG4. This galaxy shows emission-lines superposed on a steep, blue continuum with dominant flux contributions from the H II region and LMC I components (Table 4). These two stellar population elements, along with the sum of the remaining contributions from the other components are displayed in Fig. 6, together with the resulting synthesis spectrum. No reddening was found in this galaxy. The spectra in Fig. 6 are shown in their true proportions (in terms of flux fraction at $\lambda 2646 \text{ \AA}$), according to the synthesis. The case of a synthesis with large reddening is shown in Fig. 7 for G_N5860, a spectral group of distant interacting galaxies with a red continuum (Table 1). The main flux contributors for this group are the intermediate-age LMC V component (age $\approx 1.2 \text{ Gyr}$) and secondly, the young LMC I component (age $\approx 10 \text{ Myr}$, Table 4). The synthesis for each group is discussed in detail below.

The ability of the synthesis algorithm to reproduce the observed EWs of normal stellar population spectra can be evaluated by the residuals in each absorption feature, which are given in Table 5. We remind that, according to Paper I, the base ele-

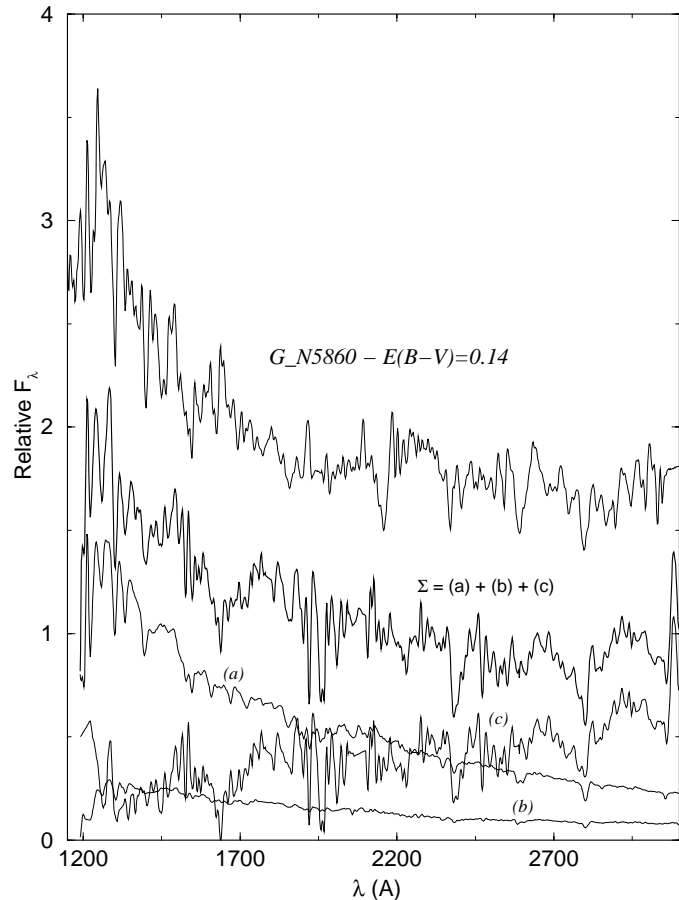


Fig. 7. Same as Fig. 6 for G_N5860, the high-reddening group of distant interacting galaxies. Components are: (a) – sum of the H II region and LMC I; (b) – sum of LMC II, LMC III and LMC IVA; (c) – sum of LMC V and E2E5.

ments with ages between 10 and 500 Myr correspond to LMC clusters, and the H II region template is an average of SMC, LMC, M 33 and M 101 H II regions, thus in general with sub-solar metallicity. In this sense, absorption features of solar and above solar-metallicity stellar populations cannot be well reproduced by our synthesis, except when the old (bulge) component is dominant. We remind again that our approach is essentially a synthesis of stellar population ages.

In the following we discuss the synthesis results for each group.

6.1. Nearby disturbed galaxy groups

ESO 338-IG4: This is a well studied blue compact galaxy with an irregular and patchy central region in which there are two nuclei separated by $\approx 3''$ (Iye et al. 1987). ESO 338-IG4 harbours an extremely blue starburst with age $\sim 7 \times 10^6$ years as well as extended systems of ionised gas (Bergvall 1985).

The UV spectrum of ESO 338-IG4 is steeper than that of G_N2782, the bluest among the luminous starburst groups studied in Paper IV. According to our stellar population synthesis, this difference is explained by a more important flux contribu-

Table 5. Equivalent Width Residuals

| Group | EW(measured) – EW(synthesis) (in Å) | | | | | | | | |
|-------------|-------------------------------------|---------------|---------------|---------------|---------------|----------------|----------------|----------------|---------------|
| | UV#4 Si II | UV#7 Si IV | UV#13 C IV | UV#19 N IV | UV#43 Fe I | UV#44 Mn II | UV#45 Fe II | UV#51 Mg II | UV#52 Mg I |
| G_N4438 | –3.55 | 2.98 | † | 5.42 | 5.96 | 5.05 | 2.69 | –1.58 | 0.36 |
| ESO 338-IG4 | 0.14 | –0.67 | 0.05 | –0.68 | 3.56 | –0.91 | 0.12 | † | † |
| G_Mrk1261 | 0.66 | –4.84 | 0.58 | –0.18: | 2.84 | 0.76 | 14.61 | –0.72 | –1.65: |
| G_Mrk1267 | 3.31 | –1.15 | 3.65 | –1.81: | 6.06 | 0.61 | –1.44 | –1.49 | 3.35 |
| G_N5860 | –1.95 | –2.02 | 1.60 | –3.94 | –5.45 | –0.14 | 0.51 | –1.96 | 6.61 |
| G_N4410 | 0.53 | –0.73 | † | –4.05: | 9.03 | 5.16 | 11.28 | 3.60 | 17.42: |
| G_Mrk54 | 0.70 | 0.27 | 0.43 | –2.18 | 2.94 | 1.75 | 2.04 | 1.20 | 4.24 |

Table notes. † – Emission line contamination.

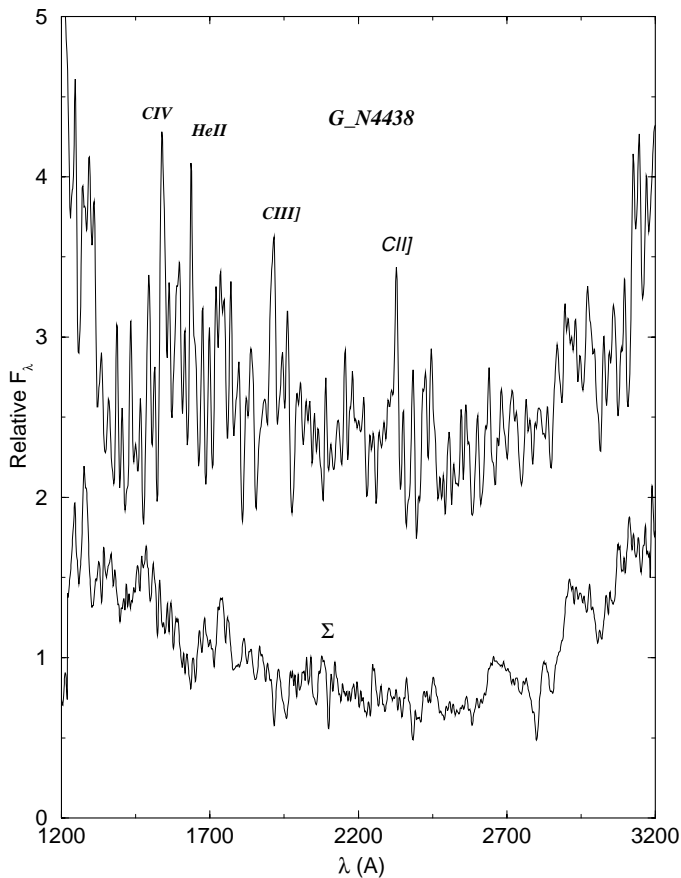


Fig. 8. Synthesis of the nearby group of disturbed galaxies G_N4438. Although the low (S/N), the presence of the old population is evident. Conspicuous emission lines are indicated.

tion from the H II region component in the former ($\approx 45\%$), and more significant contributions from evolved bursts (ages $\approx 75\text{--}200$ Myr) in the latter. The intermediate (age ≈ 1.2 Gyr) and old bulge components together contribute less than 3% of the flux at $\lambda 2646 \text{ \AA}$, while the H II region together with the LMC I components (age ≈ 10 Myr) are responsible for more than 86%, in agreement with previous results (Bergvall 1985). As can be seen in Fig. 6, ESO 338-IG4 presents conspicuous permitted emission lines such as Ly α , He II $_{\lambda 1640}$ and Mg II $_{\lambda\lambda 2796,2803}$ as

well as semi-forbidden lines such as N IV] $_{\lambda 1485}$, Si III] $_{\lambda 1682-92}$ and C III] $_{\lambda 1908}$. These emission lines are isolated and better seen after the subtraction of the stellar population continuum, as shown in Fig. 6, bottom panel. A probable mechanism for the permitted emission lines in this object is photoionisation by hot stars either young, associated with the recent starburst, or evolved post-AGBs (Binette et al. 1994); the semi-forbidden lines may originate from shock-heated gas in supernova remnants and/or winds (Sutherland et al. 1993).

G_N4438: This group contains only the galaxies ESO 383-G35, a very elongated lenticular galaxy in a cluster, and NGC 4438, which is in pair with NGC 4435 in the Virgo cluster, probably being disrupted by M 87 (Rauscher 1995); optical and near-IR integrated spectroscopy suggests that NGC 4438 might contain a low-luminosity LINER nucleus (Bonatto et al. 1989) which is further confirmed by the near-IR photometry by Jungwiert et al (1997).

Although the *IUE* spectrum of G_N4438 has a low (S/N), the presence of a bulge population can be clearly seen in Fig. 1. In fact, the population synthesis of G_N4438 shows that the old bulge population is the dominant flux contributor ($\approx 55\%$) to its spectrum, with indications of a series of important bursts distributed in age among the younger populations (Table 4). Despite the low (S/N), a few conspicuous emission lines can be seen in the spectrum of G_N4438: C IV] $_{\lambda 1549}$, He II] $_{\lambda 1640}$, C III] $_{\lambda 1908}$ and C II] $_{\lambda 2325-2329}$. They might be related to the presence of a LINER nucleus. The synthesis of G_N4438 is shown in Fig. 8.

6.2. Distant isolated galaxy groups

Groups G_Mrk1261 and G_Mrk1267 contain distant isolated, moderate-luminosity galaxies with a variety of morphological classifications such as compact, BCG and barred spirals (Table 1 and Fig. 2, bottom panel), most of which are indicative of recent star formation. For both groups, the average spatial region covered by the *IUE* slit is large (Table 2) and should encompass the bulge. Indeed, such a bulge contribution is clearly detected on the spectrum of the flat/red continuum group G_Mrk1261 (Fig. 1).

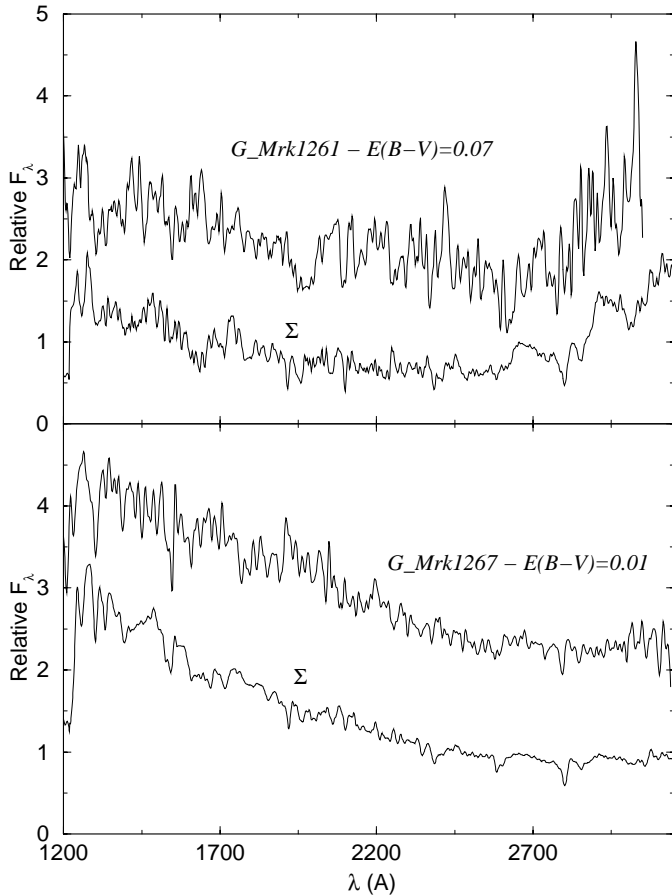


Fig. 9. Synthesis for the isolated galaxy groups. Top panel: flat/red continuum group G_Mrk1261, which presents an important contribution from the old bulge population. Bottom panel: blue continuum group G_Mrk1267. Reddening corrections have been applied with an SMC law and with $E(B - V) = 0.07$ and 0.01 respectively for G_Mrk1261 and G_Mrk1267.

G_Mrk1261: Galaxy members of this flat/red continuum group are IC 1586, a blue elliptical compact with H and K absorption lines and sharp emission lines of H I as well as $[O II]_{\lambda 3727}$, and NGC 118, a spherical compact with a blue disc (Zwicky 1971).

According to the stellar population synthesis (Table 4), the flat/red UV spectrum of G_Mrk1261 can be explained essentially by a dominant ($\approx 67\%$) flux contribution from the old bulge population and a significant contribution from the H II region component ($\approx 15\%$) together with a noticeable amount of reddening, $E(B - V) = 0.07$. The presence of enhanced star formation in the galaxies forming this group can be traced by the $\approx 31\%$ flux contribution from young components (age < 500 Myr). We emphasise, however, that G_Mrk1261, which contains isolated galaxies, is the group with the smallest flux contribution from young stellar populations among the present sample. In Fig. 9, top panel, we show the spectrum of G_Mrk1261 corrected with the SMC extinction law and $E(B - V) = 0.07$, along with the corresponding synthesis.

G_Mrk1267: The blue continuum group G_Mrk1267 includes Mrk 702 which contains three individual giant H II region complexes (Telles & Terlevich 1997) and Mrk 1267 in which Kinney et al. (1993) detected star-formation activity, in particular the presence of many early-supergiant stars.

As expected, the stellar population synthesis shows that the H II region is the dominant flux contributor to the UV spectrum of this group, while intermediate age and old bulge components together contribute up to $\approx 10\%$ only, in marked contrast with the flat/red continuum group G_Mrk1261. In terms of flux fractions, galaxies of this group are characterised by a series of star formation bursts distributed in age among the young populations. The synthesis indicates a very small reddening in the spectrum of G_Mrk1267, $E(B - V) = 0.01$, which was subsequently corrected for, using the SMC extinction law. A small contribution from the old population ($\approx 8\%$ in flux at $\lambda 2646 \text{ \AA}$) was found. The resulting synthesis and reddening-corrected spectra are displayed in Fig. 9, bottom panel.

6.3. Distant interacting galaxy groups

These groups contain galaxies in systems (pair, triple, etc) and/or with signs of interactions and even mergers, i.e. phenomena usually associated to enhanced star formation (Table 1). Observationally, their *IUE* spectra classify as red (G_N5860), blue (G_N4410) and very blue (G_Mrk54 – Fig. 2, top panel). The *IUE* slit covered similar spatial regions as in the distant isolated groups and, accordingly, it should include similar old bulge fractions.

G_N5860: Galaxy members of the red continuum group G_N5860 are NGC 5860, which is in a merging pair with fading starburst signatures (Mazzarella & Boroson 1993); NGC 2623 which is part of a well-studied triple system included in Arp's atlas of peculiar galaxies (1987) with bright tidal tails suggesting a merger, while its emission is dominated by a compact starburst (Condon et al. 1991); NGC 828 which presents a dust lane and is described as a merger with disturbed morphology (Wang et al. 1991); and Mrk 789 which has been classified as a starburst galaxy by Kukula et al. (1995).

The stellar population synthesis of this group (Table 4) shows that its dominant flux contribution is from the intermediate-age component ($\approx 58\%$) with a negligible (1%) H II region contribution. Combined with the large reddening ($E(B - V) = 0.14$), this produces the red appearance of the G_N5860 spectrum. Despite its red shape, the total flux contribution from the young populations (age < 500 Myr) still amounts to $\approx 42\%$, and is dominated by a somewhat evolved ≈ 10 Myr burst (LMC I component). Interestingly, the young populations are larger flux-contributors to this red continuum group of interacting galaxies than to the very red continuum group of isolated galaxies G_Mrk1261 (Fig. 2). This probably reinforces the existence of the link between interactions and star formation activity. The non-detection of the old bulge population in the spectrum of G_N5860 can be accounted for by dust obscura-

Table 6. Mass to light ratios

| Component | Age interval (10^9 yr) | $\frac{M}{L_{5870}}$ | $\frac{L_{5870}}{L_{2646}}$ | $\frac{M}{L_{2646}}$ |
|-----------|------------------------------|----------------------|-----------------------------|----------------------|
| RH II | 0.0–0.007 | 0.035 | 0.14 | 0.005 |
| LMC I | 0.007–0.02 | 0.007 | 0.28 | 0.002 |
| LMC II | 0.02–0.07 | 0.063 | 0.41 | 0.026 |
| LMC III | 0.07–0.2 | 0.305 | 0.65 | 0.198 |
| LMC IVA | 0.2–0.7 | 0.343 | 1.60 | 0.548 |
| LMC V | 0.7–7.0 | 2.270 | 3.00 | 6.820 |
| E2E5 | 7.0–17.0 | 8.260 | 19.10 | 157.7 |

tion, as implied by the large reddening derived in the synthesis (Table 4). The synthesis of G_N5860 (reddening-corrected with $E(B - V) = 0.14$, SMC law) is illustrated in Fig. 7. We conclude that the red appearance of these two *observed* spectra arises primarily from very different combinations in terms of reddening and stellar-population.

G_N4410: The following galaxies, members of the blue continuum group G_N4410 have been previously studied: IC 298 with a ring containing many knots of H II regions with H α emission (Horellou et al. 1995) and NGC 6090 with two compact, blue nuclei (Rakos et al. 1996).

The stellar population synthesis shows that the bluer observed spectrum of G_N4410 with respect to that of G_N5860 is due to a much smaller extinction ($E(B - V) = 0.04$) as well as to a more uniform distribution of flux contributions among the different age components (Table 4). As well, the total contribution from the young components amounts to $\approx 58\%$, a considerably larger figure than that in the red group G_N5860. The small extinction derived in the synthesis allowed the detection of a significant old bulge population contribution ($\approx 8\%$). The reddening-corrected ($E(B - V) = 0.04$, SMC law) spectrum of G_N4410 along with its corresponding synthesis are shown in Fig. 10, top panel. A few emission-lines are also present in the spectrum of G_N4410: in particular Ly α , N IV] $_{\lambda 1484}$, C IV] $_{\lambda 1549}$ and C III] $_{\lambda 1908}$. These emission lines may arise in shock-heated gas in supernova remnants and/or winds (Sutherland et al. 1993), with some photoionisation from the hot stars associated to recent starburst.

It should be noted that the stellar population syntheses of both groups G_N5860 and G_N4410 are similar to that of the nearby starburst group with flat continuum G_N3256 (Paper IV), in the sense that in all three groups there are large contributions from intermediate and young ages. Therefore, starburst activity is inferred in the mergers, and the merging time-scale should be of ~ 1 Gyr, during which most of the mass has been converted into stars (Sect. 6.4 and Table 7).

G_Mrk54: Among the members of the very blue continuum group G_Mrk54, the following galaxies have been previously studied along the lines of our analysis: Mrk 54, identified as a starburst galaxy by Glass & Brinks (1998); ESO 350-IG38

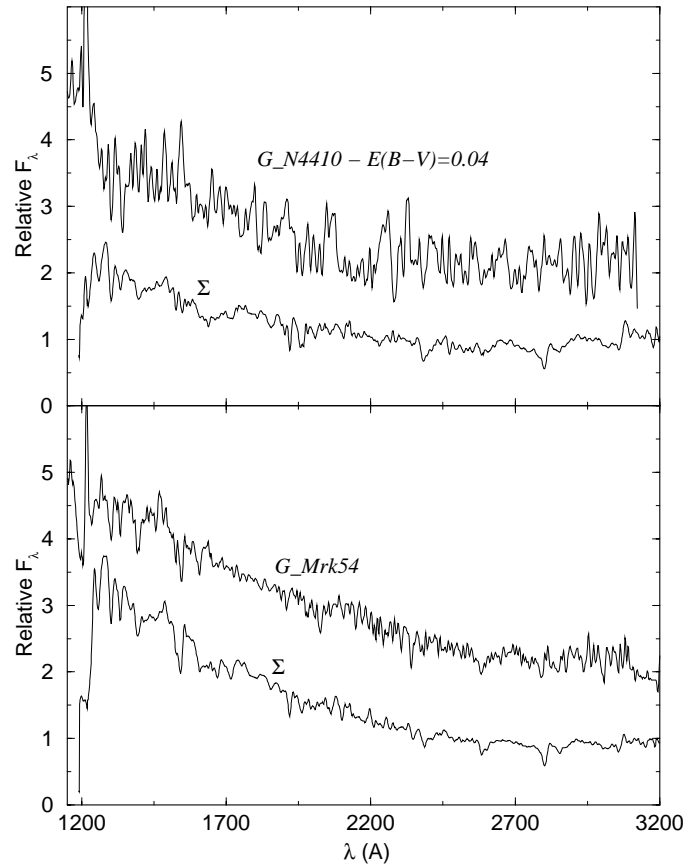


Fig. 10. Same as Fig. 9 for the groups of distant interacting galaxies with a blue continuum G_N4410 (top panel) and very blue continuum G_Mrk54 (bottom panel). The spectrum of G_N4410 has been reddening-corrected with an SMC law.

which exhibits three nuclei with emission lines typical of H II galaxies (Heisler & Vader 1994); Mrk 66 experiencing active star formation (Kinney et al. 1993); Mrk 220S in strong interaction with UGC 7905N, probably triggering the star formation activity in Mrk 220S (Kinney et al. 1993); and the now classical merger/starburst galaxy NGC 6240 which presents a disturbed morphology and a dominant contribution from supergiant stars in the H band (Lançon et al. 1996). It is worth remarking that the observed *IUE* spectrum of NGC 6240 is blue, as a member of the group G_Mrk54 (Fig. 2), while its $\lambda\lambda 3200 - 10\,000$ Å spectrum, which has been synthesised by Schmitt et al. (1996) is very red owing to high reddening. This apparent discrepancy can be explained by different optical depths probed by spectroscopy in different wavelengths. Indeed, the population synthesis in Schmitt et al. (1996) indicated a higher reddening in the near-IR range than in the near-UV range. The *IUE* spectrum of NGC 6240 supports this scenario, and in such case the present blue spectrum would correspond to an outer galaxy shell, probing the external spatial zones of the starburst. Evidence of this effect has also been found in the dust lane of Centaurus A, NGC 5128 (Storchi-Bergmann et al. 1997).

The enhanced and recent star-formation activity among galaxy members of the group G_Mrk54 implied by previous

Table 7. Synthesis results in terms of mass fractions

| Group | Mass fraction (in%) | | | | | | |
|-------------|--|-----------------|-----------------|------------------|--------------------|-------------------|------------------|
| | <i>Element:</i> <i>Age:</i> 2.5 Myr | RH II 10 Myr | LMC I 25 Myr | LMC II 75 Myr | LMC III 200 Myr | LMC IV 1.2 Gyr | LMC V ≈10 Gyr |
| G_N4438 | <0.01 | <0.01 | <0.01 | 0.01 | 0.02 | 0.26 | 99.69 |
| ESO 338-IG4 | 0.15 | 0.05 | 0.14 | 0.21 | 0.41 | 8.55 | 90.49 |
| G_Mrk1261 | <0.01 | <0.01 | <0.01 | <0.01 | 0.01 | 0.14 | 99.84 |
| G_Mrk1267 | 0.01 | <0.01 | 0.03 | 0.30 | 0.47 | 0.65 | 98.53 |
| G_N5860 | <0.01 | 0.01 | 0.04 | 0.12 | 0.20 | 99.62 | <0.01 |
| G_N4410 | <0.01 | <0.01 | 0.02 | 0.07 | 0.31 | 14.86 | 84.74 |
| G_Mrk54 | 0.01 | <0.01 | 0.01 | 0.16 | 0.18 | 0.67 | 98.96 |

studies is fully confirmed by our stellar population synthesis (Table 4). The UV flux is dominated by the H II component ($\approx 54\%$) while the intermediate and old bulge components together contribute with only $\approx 13\%$. The small reddening value derived in the synthesis allowed the detection of a significant old bulge population contribution. The bulge contribution is also found in the synthesis of Schmitt et al. (1996). According to the synthesis, the main differences between the spectrum of G_Mrk54 and that of the blue starburst ESO 338-IG4 are: a larger old population flux contribution (due to the larger spatial area sampled by the *IUE* slit) in the former, and a very important flux contribution from a 10 Myr burst in the latter. The synthesis of G_Mrk54 is shown in Fig. 10, bottom panel. Ly α and He II $_{\lambda 1640}$ in emission are clearly visible on the spectrum of G_Mrk54, and are probably resulting from photoionisation by the hot, young stars associated to the strong and recent starburst.

6.4. Mass fractions

Similarly to what has been performed in the case of the normal spiral (Paper II) and irregular galaxy groups (Paper IV), the flux fractions derived from the synthesis have been converted into mass fractions. Previously, the synthesis results in the visible/near-IR ranges (Bica 1988) had been converted into mass fractions by means of mass to light ratios M/L_V computed from a stellar evolution model of star clusters (Bica et al., 1988). Applying these results, we recall in Table 6, for each age component used in the present paper, the corresponding age interval and mass to light ratio expressed in luminosity at $\lambda 5870 \text{ \AA}$. Using the $\lambda \lambda 1000 - 10000 \text{ \AA}$ stellar population templates from Bica and collaborators (see Leitherer et al. 1996), we measured the ratio L_{5870}/L_{2646} , and derived the mass to light ratio M/L_{2646} , respectively shown in Columns 4 and 5 of Table 6. Note that small old population flux fractions in fact correspond to large mass fractions. Mass fractions for the present galaxy groups can be obtained from the synthesis flux fractions by means of M/L_{2646} . The results are shown in Table 7.

In terms of mass fractions, the old stellar population is dominant in all groups, except G_N5860 in which most of the mass is stored in the intermediate age component (Table 7). The fact that very large mass fractions are stored in the old stellar population still applies for the groups of distant interacting galaxies

G_Mrk1267 and G_Mrk54 with a blue/very blue continuum, and the nearby starburst galaxy ESO 338-IG4, despite the fact that for these three groups the stellar population synthesis shows that their UV light is strongly dominated by recent star formation (Table 4).

For the distant galaxy groups, the fact that most of the mass is stored in the old stellar population is a consequence of the large spatial region sampled by the *IUE* aperture, hence including important fractions of the old population: $\approx 9\%$ flux fraction at $\lambda 2646 \text{ \AA}$ for G_Mrk1267 and $\approx 11\%$ for G_Mrk54. Even the small fraction of old stellar population flux in ESO 338-IG4 ($\approx 0.9\%$), when converted into mass, corresponds to the dominant fraction of $\approx 90\%$. However, in the latter case of a nearby starburst galaxy, the small spatial area covered by the *IUE* aperture allowed the detection of noticeable mass fractions stored in younger populations (Table 7).

The groups containing distant interacting galaxies, with a blue continuum (G_N4410) and particularly that with a red (attenuated) continuum (G_N5860), have significant amounts of mass stored in the intermediate age population. This is probably related to the old disc contribution and/or evolved starbursts associated to early interactions.

7. Concluding remarks

This paper deals primarily with a set of relatively distant galaxies at $5000 \text{ km s}^{-1} \leq V_R \leq 16000 \text{ km s}^{-1}$ presenting enhanced star-formation. Galaxies with indication of interaction, in particular mergers, are considered separately from the isolated ones.

Rather than using individual, usually low (S/N) *IUE* spectra, the method is to group spectra of objects which share similar morphological, and primarily spectral, properties. As a consequence, high (S/N) template spectra are obtained which reflect the average properties of the corresponding galaxy members. Applying this grouping scheme, we have obtained two template spectra, i.e. groups, with the isolated galaxies and three template spectra for the interacting ones. Each group is characterised by a continuum distribution which reflects mainly a mixture of different stellar populations and a given amount of reddening.

For the sample galaxies, the average spatial area covered by the *IUE* aperture corresponds to $\approx 5 \times 10 \text{ kpc}^2$ and, conse-

quently, the observed UV spectra should contain flux contributions from a variety of stellar populations with different ages.

We analyse the stellar population content in each group spectrum by means of a synthesis algorithm which uses as a base template spectra of sub-solar metallicity star clusters for young and intermediate ages, as well as a template of metal-rich bulges of elliptical galaxies to represent the old population. As a consequence, this method is essentially a synthesis of stellar population *ages*, reproducing the basic star formation history of each individual galaxy or galaxy group. This method, in turn, does provide a quantitative measure of the star formation activity in galaxies, thus allowing comparisons to be made between interacting and isolated galaxies.

According to the synthesis, the SED of the red spectral group of interacting galaxies (G_N5860) is dominated by an intermediate age population (age ≈ 1.2 Gyr) together with a large reddening. For the isolated galaxy group with a flat/red continuum (G_Mrk1261), the SED is essentially controlled by an old population (age ≈ 10 Gyr) contribution, associated with a moderate extinction. However, the young stellar populations (age ≤ 500 Myr) appear to be larger flux contributors in the spectrum of G_N5860 (interacting galaxies) than in G_Mrk1261 (isolated galaxies), which is probably related to the interactions themselves.

Acknowledgements. We thank an anonymous referee for interesting remarks. C.B., M.G.P. and E.B. acknowledge CNPq and PRONEX/FINEP 76.97.1003.00 for partially supporting this work.

References

- Alloin D., Bica E., 1990, *Rev. Mex. Astron. Astrofis.* 21, 182
 Arp H.C., Madore B.F., 1987, *A Catalogue of Southern Peculiar Galaxies and Associations*. Cambridge University Press
 Bergvall N., 1985, *A&A* 146, 269
 Bettoni D., Buson L.E., 1987, *A&AS* 67, 341
 Bica E., Alloin D., 1987a, *A&A* 186, 49
 Bica E., Alloin D., 1987b, *A&AS* 70, 281
 Bica E., Arimoto N., Alloin D., 1988, *A&A* 202, 8
 Bica E., 1988, *A&A* 195, 76
 Bica E., Pastoriza M.G., Maia M., da Silva L.A., Dottori H., 1991, *AJ* 102, 1702
 Bica E., Bonatto C., Giovannini O., 1996, *A&AS* 119, 211
 Bica E., Bonatto C., Pastoriza M.G., Alloin D., 1996, *A&A* 313, 405
 Binette L., Magris C., Stasinska G., Bruzual A., 1994, *A&A* 292, 13
 Bonatto C., Bica E., Alloin D., 1989, *A&A* 226, 23
 Bonatto C., Bica E., Alloin D., 1995, *A&AS* 112, 71 (Paper I)
 Bonatto C., Bica E., Pastoriza M.G., Alloin D., 1996, *A&AS* 118, 89 (Paper III)
 Bonatto C., Bica E., Pastoriza M.G., Alloin D., 1998, *A&A* 334, 439 (Paper II)
 Bonatto C., Bica E., Pastoriza M.G., Alloin D., 1999, *A&A* 343, 100 (Paper IV)
 Boulanger F., Beichman C., Desert F.X., et al., 1988, *ApJ* 332, 328
 Buson L.M., Sadler E.M., Zeilinger W.W., et al., 1993, *A&A* 280, 409
 Caldwell N., 1984, *PASP* 96, 287
 Calzetti D., Kinney A.L., Storchi-Bergmann T., 1994, *ApJ* 429, 582
 Calzetti D., Bohlin R.C., Kinney A.L., Storchi-Bergmann T., Heckman T.M., 1995, *ApJ* 443, 136
 Condon J.J., Huang Z.-P., Yin Q.F., Thuan T.X., 1991, *ApJ* 378, 65
 Dahari O., 1985, *ApJS* 57, 643
 Davies R.L., Burstein D., Dressler A., et al., 1987, *ApJS* 64, 581
 Fabbiano G., Kim D.-W., Trinchieri G., 1992, *ApJS* 80, 531
 Filippenko A.V., Sargent W.L.W., 1985, *ApJS* 57, 503
 Fitzpatrick E.L., 1986, *AJ* 92, 1068
 Glass I.S., Brinks E., 1998, *A&A* 335, 152
 Green P.J., Anderson S.F., Ward M.J., 1992, *MNRAS* 254, 30
 Gregg M.D., 1989, *ApJS* 69, 217
 Heckman T.M., Balick B., Crane P.C., 1980, *A&AS* 40, 295
 Heisler C.A., Vader J.P., 1994, *AJ* 107, 35
 Helou G., 1986, *ApJ* 311, L33
 Horellou C., Casoli F., Combes F., Dupraz C., 1995, *A&A* 298, 743
 Iye M., Ulrich M.-H., Peimbert M., 1987, *A&A* 186, 84
 Jungwiert B., Combes F., Axon D.J., 1997, *A&AS* 125, 479
 Kinney A.L., Calzetti D., Bica E., Storchi-Bergmann T., 1994, *ApJ* 329, 172
 Kinney A.L., Bohlin R.C., Calzetti D., Panagia N., Wyse R.F.G., 1993, *ApJS* 86, 5
 Kukula M.J., Pedlar A., Baum S.A., O'Dea C.P., 1995, *MNRAS* 276, 1262
 Lançon A., Rocca-Volmerange B., Thuan T.X., 1996, *A&AS* 115, 253
 Leitherer C., Alloin D., Fritze-v. U., et al., 1996, *PASP* 108, 996
 Leitherer C., Robert C., Heckman T.M., 1995, *ApJS* 99, 173
 Mazzarella J.M., Boroson T.A., 1993, *ApJS* 85, 27
 Prévot M.L., Lequeux J., Maurice E., Prévot L., Rocca-Volmerange B., 1984, *A&A* 132, 389
 Rakos K.D., Maindl T.I., Schombert J.M., 1996, *ApJ* 466, 122
 Rauscher B.J., 1995, *AJ* 109, 1608
 Rosa M., Joubert M., Benvenuti P., 1984, *A&AS* 57, 361
 Schmitt H.R., Bica E., Pastoriza M.G., 1996, *MNRAS* 278, 965
 Seaton M.J., 1979, *MNRAS* 187, 73p
 Sutherland R.S., Bicknell G.V., Dopita M.A., 1993, *ApJ* 414, 510
 Storchi-Bergmann T., Kinney A.L., Challis P., 1995, *ApJS* 98, 103
 Storchi-Bergmann T., Bica E., Kinney A.L., Bonatto C., 1997, *MNRAS* 290, 231
 Telles E., Terlevich R., 1997, *MNRAS* 286, 183
 Terlevich R.J., Melnick J., Masegosa J., Moles M., Copetti M.V., 1991, *A&AS* 91, 285
 de Vaucouleurs G., de Vaucouleurs A., Corwin H.G. Jr., et al., 1991, *Third Reference Catalogue of Bright Galaxies*. Springer-Verlag, New York (RC3)
 Wang Z., Scoville N.Z., Sanders D.B., 1991, *ApJ* 368, 112
 Wood K.S., Meekins J.F., Yentis D.J., et al., 1984, *ApJS* 56, 507
 Zwicky F., 1971, In: *Catalogue of Selected Compact Galaxies and of Post-Eruptive Galaxies*. Guemligen, Switzerland